Dehydrogenation of Ethylbenzene with Nitrous Oxide in the Presence of Mesoporous Silica Materials Modified with Transition Metal Oxides

Piotr Kuśtrowski,*,† Lucjan Chmielarz,† Roman Dziembaj,† Pegie Cool,‡ and Etienne F. Vansant‡

Faculty of Chemistry, Jagiellonian University, Ingardena 3, 30-060 Krakow, Poland, and Laboratory of Adsorption and Catalysis, Department of Chemistry, University of Antwerp, Universiteitplein 1, 2610 Wilrijk, Belgium

Received: September 29, 2004; In Final Form: November 9, 2004

The novel mesoporous templated silicas (MCM-48, SBA-15, MCF, and MSU) were used as supports for transition metal (Cu, Cr, or Fe) oxides. The catalysts were synthesized using the incipient wetness impregnation, and characterized by low-temperature N_2 sorption, DRIFT, photoacoustic IR spectroscopy, UV−vis diffuse reflectance spectroscopy, and temperature-programmed desorption of ammonia. It was shown that the preparation method used results in different distributions and dimensions of the transition metal oxide clusters on the inert support surface. The prepared catalysts were tested in the reaction of oxidative dehydrogenation of ethylbenzene in the presence of nitrous oxide. The iron-containing catalysts showed the highest catalytic activity. The presence of isolated Fe^{3+} was found to be the most important factor influencing the ethylbenzene conversion. The undesirable effect of the increase in selectivity toward CO_2 was observed for the samples with the highest concentrations of acidic surface sites.

Introduction

Nitrous oxide is a very strong greenhouse gas that is responsible for various environmental problems (e.g., the destruction of the ozone layer in the stratosphere).[1] The emission of N_2O into the atmosphere caused by human activity has been growing rapidly for many years. Nowadays, it has reached a level of about 7 million tons per year.[1] The main sources of N_2O emission are the combustion of fuels (stationary and mobile), agriculture practices, wastewater treatment, and the production of adipic and nitric acids.[2,3] The decrease in N_2O emission from the chemical industry can be achieved by (i) the improvement of the currently used technologies to limit the production of N_2O, (ii) the catalytic decomposition of N_2O, (iii) the catalytic reduction of N_2O, or (iv) the use of N_2O as a chemical reactant. Nitrous oxide can be applied as a mild oxidizing agent in selective oxidation of hydrocarbons. Suzuki et al.[4] described the performance of N_2O in a direct hydroxylation of benzene to phenol on H−ZSM-5. It was shown[5] that iron complexes stabilized in a ZSM-5 matrix can transform N_2O into surface α-oxygen species, which are extremely active in the process of benzene hydroxylation. This finding enabled the application of ZSM-5 type zeolites in the commercialized technology of phenol production by benzene hydroxylation in the presence of N_2O. In this case, nitrous oxide is obtained from flue gases of adipic acid manufacture containing more than 20% of N_2O. Furthermore, the use of N_2O in some other oxidation reactions, e.g., partial oxidation of ethane to ethylene and acetaldehyde over supported molybdenum[6] and vanadium[7] catalysts, and in the oxidative dehydrogenation of *n*-butane using MgO-supported vanadium oxide catalysts,[8] is mentioned in the literature. Recently, Kuśtrowski et al.[9] showed that nitrous oxide can also be used as an oxidant in the process of oxidative dehydrogenation of ethylbenzene to styrene.

Nowadays, styrene is commercially produced by dehydrogenation of ethylbenzene over potassium-doped hematite catalysts at 550−650 °C. Introduction of additional promoters (e.g., Cr, Ce) to the hematite-based catalyst resulted in a styrene selectivity higher than 95%. Due to thermodynamic limitations and highly endothermic effect, the ethylbenzene dehydrogenation is performed in the presence of an overheated water steam. H_2O is used at about 10 times higher molar amount compared to ethylbenzene vapor. Oxidative dehydrogenation of ethylbenzene was proposed as an alternative route in styrene production.[10−12] Because of the exothermal effect of the oxydehydrogenation, a higher conversion of ethylbenzene at significantly lower temperatures can be obtained compared to that in a classical dehydrogenation process. Apart from oxygen, which is the most frequently studied oxidizing agent, other oxidants (e.g., SO_2, nitrobenzene, N_2O) were also tested in the oxidative dehydrogenation of ethylbenzene. However, the use of SO_2 was connected with the formation of toxic byproducts.[13] The simultaneous and mutual reactions of ethylbenzene dehydrogenation and nitrobenzene hydrogenation proceed with a low efficiency.[14] Superior results were obtained by coupling the N_2O decomposition with the ethylbenzene dehydrogenation over γ-Al_2O_3-supported transition metal oxide catalysts.[9] The most promising catalysts were based on copper, iron, and chromium oxide containing materials.

In this study a detailed investigation of ethylbenzene dehydrogenation with N_2O using mesoporous silica materials modified with copper, iron, and chromium oxides was carried out. Different calcined mesoporous templated silicas (MCM-48, SBA-15, MCF, and MSU) were used as support materials. Furthermore, a detailed characterization of the catalysts was performed using BET method, Fourier transform infrared spectroscopy (FTIR), UV−vis diffuse reflectance spectroscopy

* To whom correspondence should be addressed. Telephone: +48 12 6632006. Fax: +48 12 6340515. E-mail: kustrows@chemia.uj.edu.pl.
† Jagiellonian University.
‡ University of Antwerp.

10.1021/jp0455881 CCC: $30.25
Published on Web 12/24/2004

(UV−vis-DRS), and temperature-programmed desorption of ammonia (NH_3-TPD), allowing determination of their structural, textural, and acidic properties.

Experimental Section

Catalyst Preparation. Four different silica-based mesoporous materials (MCM-48, SBA-15, MCF, and MSU) were used as a support for the transition metal oxides. MCM-48 was prepared using the Gemini 16-12-16 surfactant dissolved in an aqueous solution of NaOH.[15] Fumed silica (Aerosil 380) was added after 0.5 h. The amount of reactants used was adjusted to obtain the molar ratio of $Si/OH^-/H_2O$/surfactant = 1/0.26/100/0.1. The resulting gel was transferred into an autoclave and aged at 100 °C for 3 days. Then it was separated by filtration, washed with 15 mL of distilled water, and resuspended in distilled water for 24 h at 100 °C. This procedure was repeated once more. The final product was filtered, washed with distilled water, and dried at room temperature.

The synthesis procedure of SBA-15 was described earlier by Van Bavel et al.[16] A sample of 4 g of poly(ethylene oxide)-*block*-poly(propylene oxide)-*block*-poly(ethylene oxide) triblock copolymer (Pluronic P123) was dissolved in 2 M HCl. Subsequently, 9.14 mL of tetraethyl orthosilicate (TEOS) was added. The obtained suspension was stirred at 45 °C for 8 h and then aged at 80 °C for 15 h. The product was filtered, washed with distilled water, and dried at room temperature.

MCF was prepared according to the procedure reported by Schmidt-Winkel et al.[17] A sample of 4 g of Pluronic P123 was dissolved in 150 mL of an aqueous solution of HCl (1.6 M) at 35−40 °C. Then, NH_4F (46.7 mg) and 1,3,5-trimethylbenzene (2.0 g) were added under vigorous stirring. After 1 h, TEOS (9.14 mL) was added. After 20 h at 35−40 °C, the slurry was transferred to an autoclave and aged at 100 °C for 24 h. The obtained precipitate was filtered, washed with distilled water, and dried in air.

The synthesis of MSU was performed using the modified procedure given by Kim et al.[18] Sodium silicate (11.8 mL) was dissolved in 278 mL of distilled water and mixed with 0.22 M Brij 56 (5.5 mL) and acetic acid (2.5 mL). After 1 h, NaF (0.06 g) was added, and the resulting gel was left at 60 °C for 3 days under vigorous stirring. Finally, the white product was filtered, washed with distilled water, and dried at room temperature.

The synthesized silica-based supports were calcined at 550 °C with a heating rate of 1 °C/min and an isothermal period of 8 h in air atmosphere. Supported catalysts were prepared by an impregnation technique using solutions of $Cu(NO_3)_2 \cdot 3H_2O$, $Fe(NO_3)_3 \cdot 9H_2O$, and $Cr(NO_3)_3 \cdot 9H_2O$. All metal nitrates used were supplied from Fluka. The amount of salts was adjusted to obtain a transition metal content in the catalysts equal to 3.0. The obtained precursors were dried at room temperature for 3 days and then calcined in air at 450 °C for 3 h.

Characterization Techniques. Transition metal loadings were determined by electron microprobe analysis performed on a JEOL Superprobe 733. Textural parameters of the catalysts were determined by N_2 sorption at −196 °C using an ASAP 2010 (Micromeritics) after outgassing the samples at 350 °C under vacuum. The total pore volume was calculated and the pore size distribution was obtained using the Barret−Joyner−Halenda (BJH) method. The micropore volume was calculated by the *t*-plot analysis. DRIFT spectra were recorded on a Nicolet 20SXB FTIR spectrometer equipped with a Spectra-Tech diffuse reflectance accessory. The resolution was 4 cm^{-1} and 200 scans were collected for a 2 wt % diluted sample in KBr. Photoacoustic IR spectroscopy (PAS) was performed on a Nexus spectrometer bench placed in an ultradry air box and equipped with an MTEC 300 PA detection cell flushed with zeolite-dried helium. Usually 2000 scans were taken with a resolution of 4 cm^{-1}. UV−vis diffuse reflectance (UV−vis-DRS) analysis was carried out on a Nicolet Evolution 500 spectrophotometer. The spectra were taken in the range of 200−800 nm for the samples (2 wt %) diluted in KBr.

The surface concentration of acidic centers was determined by temperature-programmed desorption of ammonia (NH_3-TPD). Experiments were typically carried out in the temperature range of 70−600 °C in a fixed-bed flow microreactor. The temperature of the reactor was measured by a K-type thermocouple located in a quartz capillary immersed in the sample bed. The desorbing molecules were monitored on-line by a VG QUARTZ quadrupole mass spectrometer (QMS) connected directly to the reactor outlet via a heated line. Before the TPD experiments, the catalyst (50 mg) was outgassed at 550 °C for 15 min in a flow of helium (20 mL/min). Subsequently, the sample was cooled to 70 °C and saturated in a flow of gas mixture containing 1 vol % NH_3 in helium (20 mL/min) until no further adsorption was observed. Then the sample was purged in a He flow until a constant baseline level was attained. Desorption was carried out with a linear heating rate (10 °C/min) in a flow of He (20 mL/min). Traces of H_2O and O_2 in the pure helium (grade 5.0) used as the eluant gas were removed by appropriate traps (Alltech). NH_3-TPD spectra were obtained from the $m/z = 16$ mass-to-charge signal ratio after a calibration with commercial test mixtures.

Catalytic Tests. Catalytic runs were performed in a plug flow microreactor (i.d., 6.0 mm; length, 240 mm). A sample of 50 mg of the catalyst was loaded at the central position of the reactor onto a quartz wool plug. The flow of the gaseous reactants was controlled by mass flow controllers (Brooks 5850E). Ethylbenzene was fed into the system with a syringe pump (Cole-Parmer). The reaction products were monitored by a gas chromatograph (Varian CP-3800) equipped with three capillary columns—CP-8 (for separation of aromatic compounds), Poraplot Q (for CO_2, H_2O, N_2O), and Molsieve 5A (for N_2, O_2, CO)—and two detectors—TCD and mass spectrometer Saturn 2000 (Varian). A sample of reactants was always collected directly from the outlet of the reactor using a six-port valve (Valco).

The activity of the mesoporous catalysts was studied for the decomposition of nitrous oxide as well as for the oxidative dehydrogenation of ethylbenzene in the presence of N_2O. Prior to the catalytic run the sample was outgassed at 450 °C for 30 min in a flow of N_2O (0.4 mL/min) diluted with He (up to a total flow of 49.6 mL/min). Then dosing of ethylbenzene (130 μL of liquid ethylbenzene per hour) started in the case of the dehydrogenation reaction. The first GC analysis was performed after 25 min. The temperature of the catalyst bed was increased from 450 to 550 °C in steps of 50 °C with three analyses of the obtained products (at 35 min intervals) at each step.

Results and Discussion

Chemical Composition and Textural Parameters. The content of transition metals in the samples after impregnation followed by thermal treatment is shown in Table 1. The textural parameters of the studied samples are summarized in Table 2. It is obvious that the parent mesoporous materials vary in specific surface area, micropore volume, mesopore volume, and pore size distribution. Furthermore, an introduction of transition metal oxides to the parent mesoporous samples resulted in a decrease of their surface area and porosity. This effect is very

TABLE 1: Transition Metal Loading of the Studied Catalysts

	total content of transition metal [wt %]	content of different forms of metal ions [wt %]	
		isolated Fe^{3+}	Fe^{3+} clusters
Fe−MCF	2.5	1.4	1.1
Fe−MSU	5.4	2.8	2.6
Fe−MCM-48	3.8	1.8	2.0
Fe−SBA-15	2.7	1.3	1.4

	total content of transition metal [wt %]	content of different forms of metal ions [wt %]	
		Cr^{3+} species	Cr^{6+} species
Cr−MCF	2.4	0.2	2.2
Cr−MSU	4.5	0.0	4.5
Cr−MCM-48	4.0	0.8	3.2
Cr−SBA-15	3.1	0.2	2.9

	total content of transition metal [wt %]	content of different forms of metal ions [wt %]			
		Cu^{+} species	isolated Cu^{2+}	Cu^{2+} clusters	bulk CuO
Cu−MCF	4.1	1.5	1.5	1.0	0.1
Cu−MSU	5.3	1.4	0.5	3.1	0.3
Cu−MCM-48	2.8	2.2	0.2	0.4	0.0
Cu−SBA-15	3.8	1.3	1.6	0.8	0.1

TABLE 2: Textural Parameters of Transition Metal Modified Mesoporous Catalysts

sample	S_{BET} [m^2/g]	V_{micro} [cm^3/g]	V_{total} [cm^3/g]	av pore diam [Å]
MCF	638	0.11	2.27	308
Cu−MCF	527	0.04	1.42	233
Fe−MCF	566	0.07	1.64	234
Cr−MCF	549	0.06	1.71	260
MSU	206	0	0.61	153
Cu−MSU	185	0	0.60	130
Fe−MSU	189	0	0.60	130
Cr−MSU	190	0	0.59	130
MCM-48	1115	0	1.05	30
Cu−MCM-48	1007	0	0.90	27
Fe−MCM-48	1050	0	0.97	30
Cr−MCM-48	1054	0	0.96	30
SBA-15	580	0.10	0.61	56
Cu−SBA-15	499	0.07	0.54	56
Fe−SBA-15	535	0.09	0.55	56
Cr−SBA-15	518	0.08	0.55	56

significant for the Cu-containing materials. Modification of the mesoporous silicas with copper resulted in a loss of 10% (for Cu−MSU and Cu−MCM-48), 14% (for Cu−SBA-15), or 17% (for Cu−MCF) of their initial surface area, and 3% (for Cu−MSU), 11% (for Cu−SBA-15), 14% (for Cu−MCM-48), or even 37% (for Cu−MCF) of total pore volume. Similar changes in textural parameters were also detected for the Cr- and Fe-rich catalysts. It should be therefore assumed that modification of the mesoporous silicas with transition metal oxides resulted in differences in distribution and dimensions of the transition metal oxide clusters.

DRIFT and Photoacoustic Spectroscopy. The infrared spectra of the parent samples show bands typical for mesoporous silica materials. However, a sharp distinct band at 3740−3750 cm^{-1}, attributed to isolated silanol groups, was observed. A broad band in the range from 3000 to 3700 cm^{-1} can be assigned to hydrogen-interacting silanols. Moreover, at lower frequencies very intense bands corresponding to the asymmetric stretching vibration of strained siloxane bridges (about 1230 cm^{-1}) and silicate (around 1050−1100 cm^{-1}) were found.

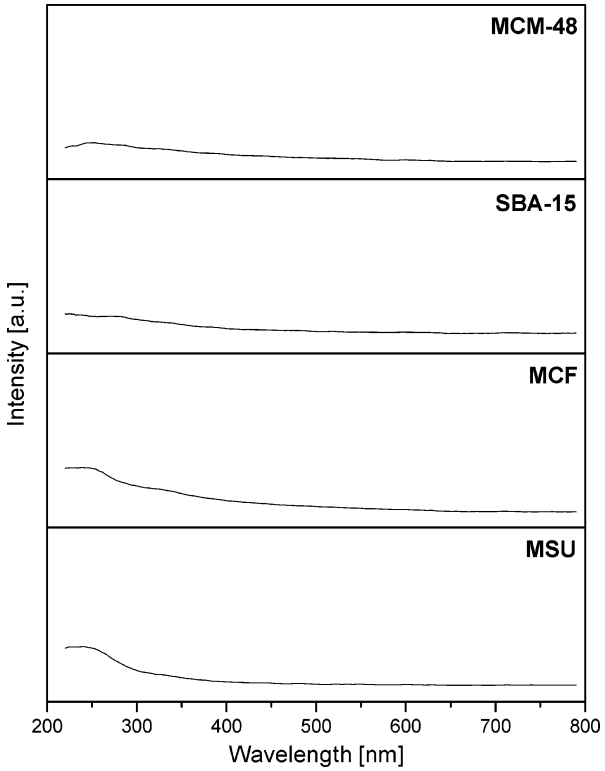

Figure 1. UV−vis diffuse reflectance spectra of pure supports.

The modification of silica supports with transition metals oxides did not cause essential changes in the infrared spectra. Therefore, it can be assumed that during an impregnation followed by a calcination process no interaction between surface silanol groups and metal oxide occurred. It should be therefore stated that silica-type supports are inert in relation to active transition metal oxide phase. However, in the spectra of samples modified with chromium, an intense band at about 940 cm^{-1} appeared typical for the presence of chromates.

UV−Vis-DRS. Diffuse reflectance UV−vis spectra were recorded for all samples to characterize the coordination environment of introduced transition metals. The spectra of the parent silica-based supports show only a very weak band centered at 250−270 nm attributed to structural Si in tetrahedral coordination (Figure 1). An introduction of iron resulted in an appearance of three new bands, as is shown in Figure 2A. Two intense bands, which can be assigned to the $d\pi-p\pi$ charge transfer between iron and oxygen atoms, are observed at low wavelengths. The band between 200 and 300 nm corresponds to isolated Fe^{3+} species, whereas the band in the range of 300−450 nm can be attributed to small oligonuclear $(FeO)_n$ species.[19−21] Moreover, a very broad and relatively weak band can be distinguished in the range of 350−550 nm. This band is assigned to symmetrical and spin-forbidden d−d transitions of Fe^{3+}.[22] It should be noticed that the relation between the amount of isolated and oligonuclear species, estimated on the basis of determined peak areas, varies for the investigated Fe-containing catalysts (cf. Table 1). Fe−MCF consists of the relatively highest amount of isolated Fe^{3+} ions (56.0%). The Fe−MSU, Fe−SBA-15, and Fe−MCM-48 catalysts show 51.9, 47.4, and 48.1% Fe in the form of separate Fe^{3+} species.

The spectra of the Cu-containing catalysts are illustrated in Figure 2B. They consist of at least four maxima showing very complex nature in the Cu coordination in the samples. It should be noted that the band observed at low wavelengths, below 250 nm, can suggest the presence of Cu^{+} species on the sample

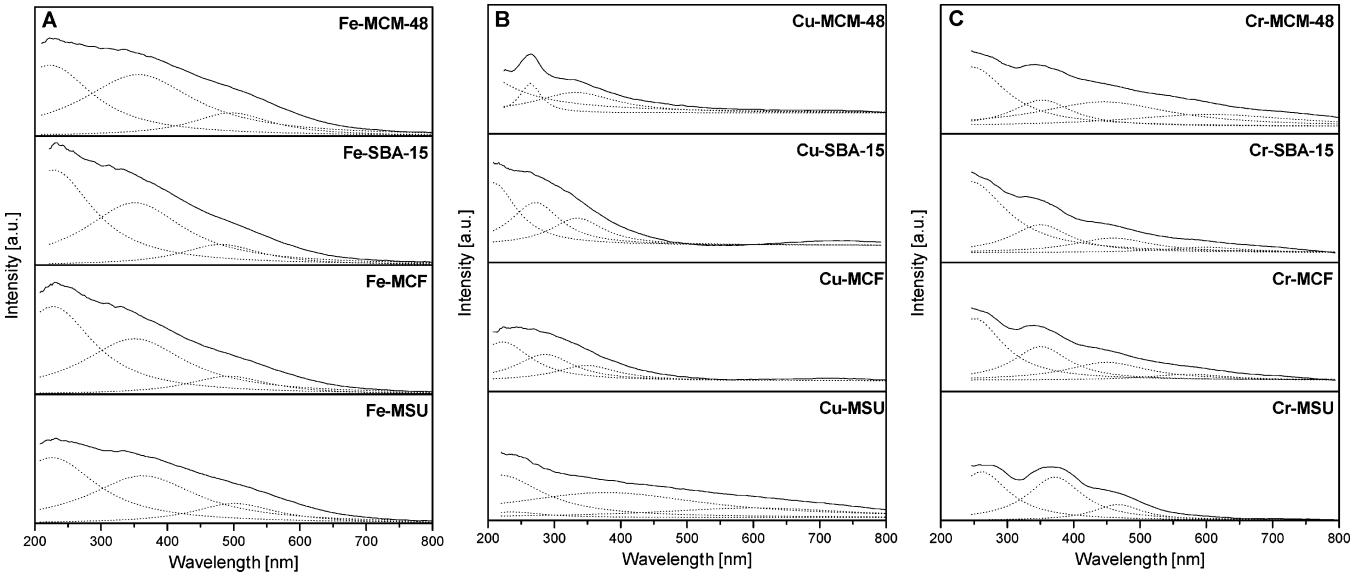

Figure 2. UV−vis diffuse reflectance spectra of silica-based samples modified with oxides of Fe (A), Cu (B), and Cr (C).

surface.[23] However, a majority of copper exists in a form of Cu^{2+} ions. The band centered at 270−280 nm can be attributed to the charge transfer between mononuclear Cu^{2+} and oxygen, whereas the band at around 330−350 nm corresponds to the presence of $[Cu-O-Cu]_n$-type clusters over the support surface.[24−26] Moreover, the band observed in the region between 530 and 800 nm can be attributed to the d−d transition of Cu with octahedral environment in CuO.[27,28] Deconvolution of DRS peaks revealed that Cu−SBA-15 consists of the highest amount of well-dispersed copper among the different samples (cf. Table 1). On the contrary, the MSU-supported copper oxide catalyst is characterized by the presence of the largest amount of Cu^{2+} bulky CuO species.

In Figure 2C the UV−vis-DRS spectra of Cr-modified mesoporous sieves are given. For the different samples two strong bands at 260−280 and 330−350 nm, which are characteristic of the presence of Cr^{6+}, were detected.[29] The appearance of Cr^{6+} in the samples obtained by impregnation with chromium(III) nitrates followed by calcination shows that during the thermal treatment an oxidation of Cr^{3+} cations occurred. The band around 470 nm, ascribed to Cr^{6+} present in chromate or dichromate arrangement being in contact with the support (symmetry forbidden in the T_d coordination), is also observed.[30] The formation of surface chromates was confirmed by the results of photoacoustic spectroscopy. The Cr−MCF, Cr−MCM-48, and Cr−SBA-15 catalysts show additionally bands at 450−460 nm ($A_{2g} \rightarrow T_{1g}$) and 580−600 nm ($A_{2g} \rightarrow T_{2g}$), typical for octahedrally coordinated Cr^{3+} systems. For the Cr−MSU sample the calcination results in a complete oxidation of Cr^{3+} cations, and therefore bands at 450−460 and 580−600 nm are not found.

Surface Acidity. Due to a possible influence of the surface acidity on the catalytic activity, the catalysts were examined by temperature-programmed desorption of NH_3 in order to determine the total concentration of acidic sites present on the catalyst surface. The collected results are summarized in Table 3. Among the parent materials the highest amount of chemisorbed ammonia was measured for the MCF sample. Significantly lower NH_3 desorptions for MSU and SBA-15 were observed, while MCM-48 shows a complete absence of acidic surface sites. Probably the basic conditions which were applied in the preparation of MCM-48 material resulted in the absence of acidic centers.

TABLE 3: Surface Acidity of the Studied Catalysts

	concentration of acidic sites	
sample	[μmol NH_3/g_{cat}]	[μmol NH_3/m^2_{cat}]
MCF	54.7	0.086
Cu−MCF	62.6	0.119
Fe−MCF	81.2	0.143
Cr−MCF	24.7	0.045
MSU	8.8	0.043
Cu−MSU	27.9	0.151
Fe−MSU	23.8	0.126
Cr−MSU	36.6	0.193
MCM-48	0.0	0.000
Cu−MCM-48	72.8	0.072
Fe−MCM-48	24.1	0.023
Cr−MCM-48	51.1	0.048
SBA-15	8.5	0.015
Cu−SBA-15	413.9	0.829
Fe−SBA-15	74.0	0.138
Cr−SBA-15	122.5	0.236

The amount of desorbed NH_3 increased considerably when transition metal oxides were introduced to the silica-based mesoporous materials. This effect can be explained by the presence of acceptor properties for the free electron pair of ammonia due to the unoccupied d orbitals of transition metals. The highest quantity of chemisorbed ammonia was detected for the Cu−SBA-15 sample. Nevertheless, no clear correlation between the nature of the transition metal oxides and the acidity of catalyst was found.

Catalytic Activity. The activated mesoporous materials were tested as catalysts for the decomposition of nitrous oxide. The collected results are shown in Figure 3. In all the catalytic runs only N_2 and O_2 were observed among the reaction products. Both the Cr- and Fe-containing samples showed a very poor catalytic performance. In the case of the Cr−silica-based mesoporous sieves the activity of catalysts did not exceed 5% in the temperature range of 450−550 °C. For the Fe samples only Fe−MCM-48 showed a N_2O conversion of 8% at 550 °C. Significantly better catalytic results were obtained for the Cu-containing samples. An influence of the type of support on the

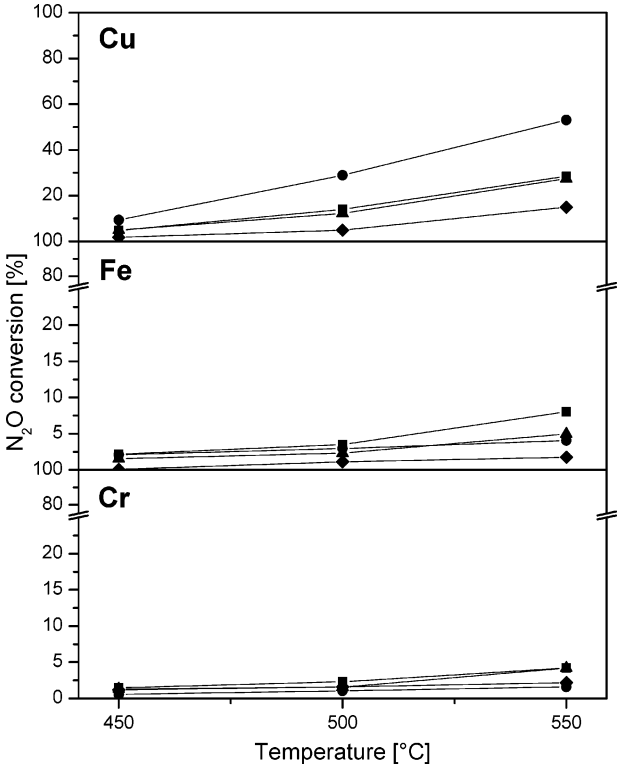

Figure 3. N_2O conversion vs reaction temperature measured for decomposition of N_2O over transition metal oxide modified MCM-48 (■), SBA-15 (●), MCF (▲), and MSU (◆) mesoporous catalysts.

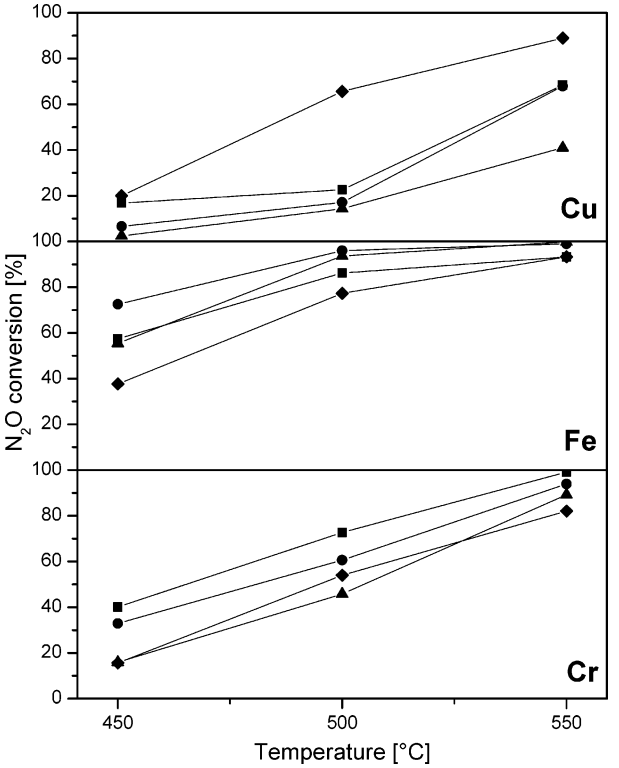

Figure 4. N_2O conversion vs reaction temperature measured for oxidative dehydrogenation of ethylbenzene in the presence of N_2O over transition metal oxide modified MCM-48 (■), SBA-15 (●), MCF (▲), and MSU (◆) mesoporous catalysts.

activity of catalyst was observed in this case. The Cu samples show the following activity sequence:

$$\text{Cu}-\text{SBA-15} > \text{Cu}-\text{MCM-48} \sim \text{Cu}-\text{MCF} > \text{Cu}-\text{MSU}$$

The conversion of nitrous oxide can be considerably increased when the N_2O decomposition process is coupled with the reaction of an alkane dehydrogenation. The effectiveness of ethylbenzene, as a "N_2O reductant", is presented in Figure 4, illustrating the observed conversion of nitrous oxide in the presence of ethylbenzene. The enhancement of the N_2O decomposition was the lowest for the Cu-containing samples, which were the most active in the decomposition of nitrous oxide performed without using an alkane. A higher effect of coupling both processes was found for the Cr- and Fe-containing samples; however, the most promising results were obtained over silica-based mesoporous material supported iron oxide. At a reaction temperature as low as 450 °C, the conversion of N_2O ranged from 37.7% (for Fe−MSU) to 72.5% (for Fe−SBA-15). Raising the reaction temperature resulted in an increase of the N_2O conversion, which reached a level above 90% at 550 °C for all Fe-containing catalysts.

The coupling of N_2O decomposition and ethylbenzene dehydrogenation has a potential industrial importance due to the possibility of decreasing the N_2O concentration, N_2O being one of the recognized greenhouse gases, as well as the conversion of ethylbenzene to styrene polymerization processes. Therefore, a catalyst with a high activity in conversion of ethylbenzene and a selectivity toward styrene is important. The results of the ethylbenzene conversion obtained in the coupling of N_2O decomposition and ethylbenzene dehydrogenation for various transition metal oxide modified mesoporous sieves are shown in Figure 5. Among the tested catalysts the Fe-containing samples showed the highest conversion of ethylbenzene. At 450 °C the activity of all the tested Fe catalysts was similar (13.3−18.4%). A significant difference in the catalytic activity was observed with increasing reaction temperature. The Fe-contain-

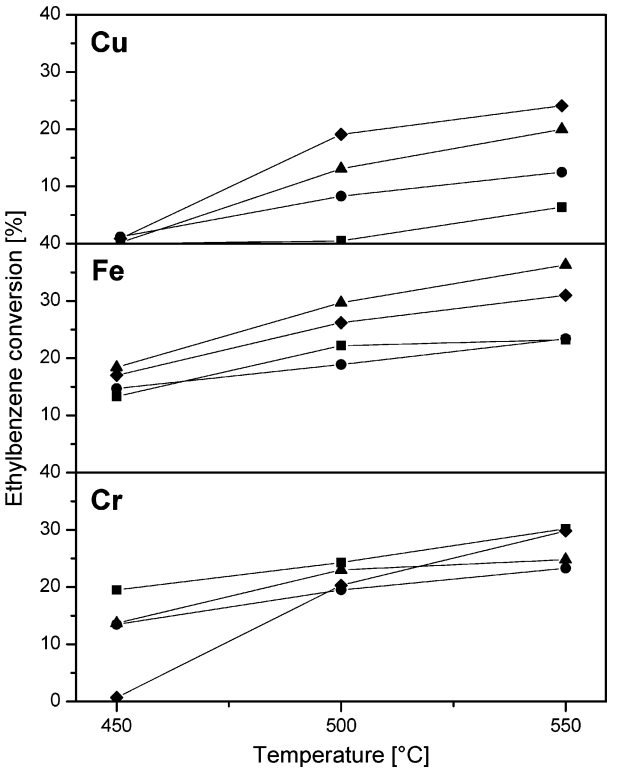

Figure 5. Ethylbenzene conversion vs reaction temperature measured for oxidative dehydrogenation of ethylbenzene in the presence of N_2O over transition metal oxide modified MCM-48 (■), SBA-15 (●), MCF (▲) and MSU (◆) mesoporous catalysts.

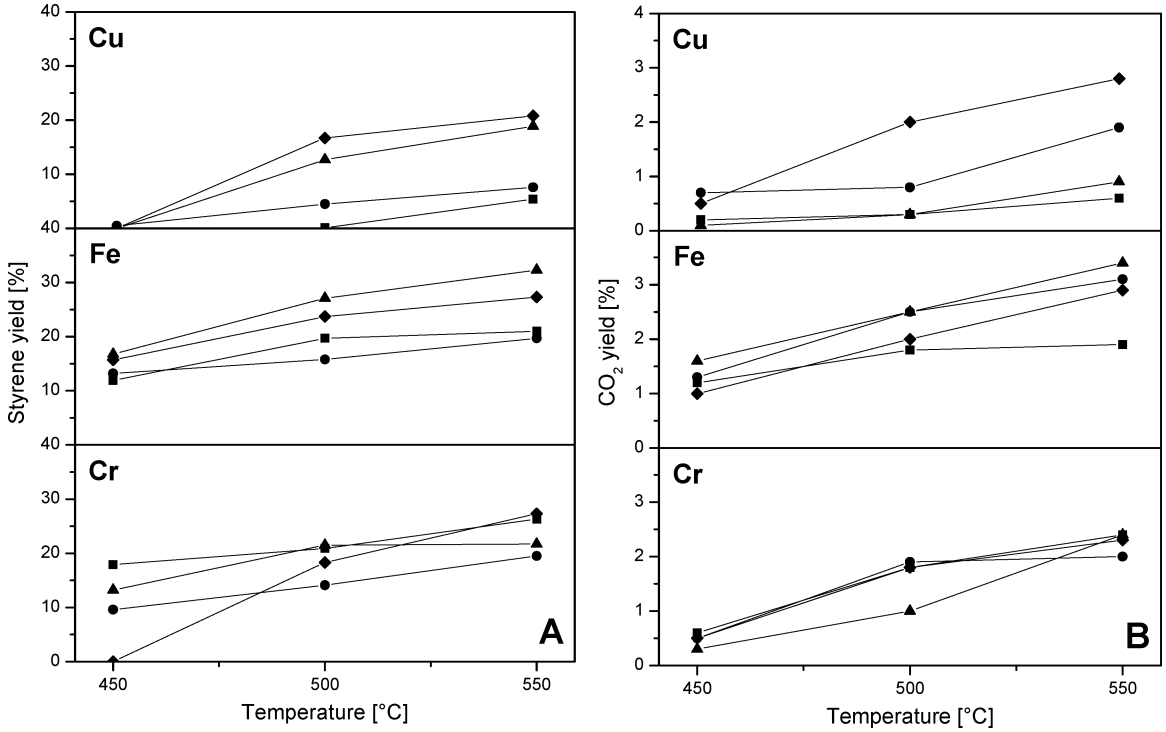

Figure 6. Styrene (A) and CO_2 (B) yields vs reaction temperature measured for oxidative dehydrogenation of ethylbenzene in the presence of N_2O over transition metal oxide MCM-48 (■), SBA-15 (●), MCF (▲), and MSU (◆) mesoporous catalysts.

TABLE 4: Selectivities toward Styrene and CO_2 over the Most Active Fe-Containing Samples at Different Reaction Temperatures

	selectivity to styrene			selectivity to CO_2		
catalyst	450 °C	500 °C	550 °C	450 °C	500 °C	550 °C
Fe−MCM-48	89.5	88.7	90.5	9.0	8.1	8.2
Fe−SBA-15	89.8	83.6	84.2	8.8	13.2	13.2
Fe−MCF	91.3	91.2	89.0	8.7	8.4	9.4
Fe−MSU	92.4	90.5	88.1	5.9	7.6	9.4

ing catalysts can be ordered with respect to their activity in the ethylbenzene conversion as follows:

$$\text{Fe−MCF} > \text{Fe−MSU} > \text{Fe−MCM-48} > \text{Fe−SBA-15}$$

No significant decrease in the activity was observed during the catalytic runs. It should be therefore assumed that nitrous oxide protects the catalyst against formation of inactive carbonaceous deposit.

The obtained catalytic results are well correlated with the UV−vis-DRS data which allowed us to distinguish the mono- and oligonuclear species of iron present in the catalysts. The Fe−MCF sample with the highest ratio between separate and oligonuclear iron ions (56.0%) was the most active in the ethylbenzene dehydrogenation. Fe−MSU, which consists of 51.5% isolated Fe^{3+} cations, was slightly less active. The lowest catalytic activity was obtained for the Fe−MCM-48 and Fe−SBA-15 samples containing the relatively lowest content of isolated iron species. Hence, it should be assumed that the dispersion of iron seems to be a crucial parameter influencing the catalytic performance of the Fe-containing mesoporous sieves in the dehydrogenation of ethylbenzene in the presence of N_2O.

In the catalytic reaction of ethylbenzene dehydrogenation in the presence of nitrous oxide, mainly styrene, as a desirable product, and CO_2, as a byproduct, were produced. The formation of only traces of other aromatic hydrocarbons (such as benzene and toluene) as well as CO was detected. Among the tested catalysts the highest yield of styrene, as is shown in Figure 6A, was observed for the samples containing iron. In the presence of the most active Fe−MCF sample a styrene yield of 32.3% was achieved at 550 °C. It should, moreover, be added that the Fe samples showed a high selectivity toward styrene (Table 4). However, the Fe catalysts are also characterized by the highest activity in burning aromatics to CO_2 (cf. Figure 6B). The sequence in catalyst performance with respect to their activity for the formation of carbon dioxide differs from that observed for the ethylbenzene conversion and styrene yield:

$$\text{Fe−MCF} > \text{Fe−SBA-15} > \text{Fe−MSU} > \text{Fe−MCM-48}$$

Therefore, we can conclude that not only dispersion of iron is important but also the surface acidity plays a dominant role in the oxidation of aromatics. From NH_3-TPD it was obvious that the Fe−MCF sample showed the highest concentration of acidic sites among the Fe-containing catalysts.

Conclusions

Transition metal oxides, introduced by the incipient wetness technique, into mesoporous templated silicas (SBA-15, MCF, MCM-48, and MSU) form different surface species. UV−vis-DRS measurements revealed that in the Fe-modified silica-based catalysts iron exists in a form of both isolated Fe^{3+} and oligonuclear $(FeO)_n$ species. For the Cu-containing samples, the formation of Cu^{+}, mononuclear Cu^{2+}, $[Cu−O−Cu]_n$-type clusters, and CuO crystals was observed. Calcination of the samples modified with Cr at elevated temperature resulted in

oxidation of Cr^{3+} to Cr^{6+} present in chromate or dichromate arrangement that was shown by the results of FTIR and UV−vis-DRS studies. On the other hand, the NH_3-TPD experiments showed that the acidity of silica-based materials significantly increased after the introduction of transition metal oxides.

The transition metal (Cu, Fe, or Cr) oxide containing mesoporous silicas showed rather poor catalytic activity in the N_2O decomposition. The conversion of nitrous oxide significantly increased when ethylbenzene was introduced to the reaction system. Nitrous oxide was found to be an oxidant, which can efficiently transform ethylbenzene to styrene. The best catalytic results for the coupling of N_2O decomposition with ethylbenzene dehydrogenation were achieved over the Fe-containing catalysts. It was observed that the conversion of ethylbenzene is strictly correlated with the dispersion of iron. The highest catalytic activity was found for the samples containing the relatively highest amount of isolated Fe^{3+} species. Apart from styrene, CO_2 was formed as a side product in the oxidative dehydrogenation of ethylbenzene in the presence of N_2O. It should, however, be noticed that selectivity toward CO_2 depends strongly on the surface acidity.

Acknowledgment. The authors thank the Ministry of Flanders and the Polish Ministry of Scientific Research and Information Technology for financial support in the frame of bilateral Flemish−Polish project for 2004−2005.

References and Notes

(1) Wojtowicz, M. A.; Pels, J. R.; Moulijn, J. A. *Fuel Process. Technol.* **1993**, *34*, 1.
(2) Kapteijn, F.; Rodriguez-Mirasol, J.; Moulijn, J. A. *Appl. Catal. B* **1996**, *9*, 25.
(3) Reimer, R. A.; Slaten, S. C.; Seapan, M.; Lower, M. W.; Tomlinson, P. E. *Environ. Prog.* **1994**, *13*, 134.
(4) Suzuki, E.; Nakashiro, K.; Ono, Y. *Chem. Lett.* **1988**, 953.
(5) Panov, G. I.; Uriarte, A. K.; Rodkin, M. A.; Sobolev, V. I. *Catal. Today* **1998**, *41*, 365.
(6) Mendelovici, L.; Lunsford, J. H. *J. Catal.* **1985**, *94*, 37.
(7) Erdöhelyi, A.; Solymosi, F. *J. Catal.* **1991**, *129*, 497.
(8) López Nieto, J. M.; Dejoz, A.; Vazquez, M. I.; O'Leary, W.; Cunningham, J. *Catal. Today* **1998**, *40*, 215.
(9) Kuśtrowski, P.; Zbroja, M.; Dziembaj, R.; Papp, H. *Catal. Lett.* **2002**, *80*, 1.
(10) Emig, G.; Hofmann, H. *J. Catal.* **1983**, *84*, 15.
(11) Cavani, F.; Trifirò, F. *Appl. Catal. A* **1995**, *133*, 219.
(12) Lisovskii, A. E.; Aharoni, C. *Catal. Rev.—Sci. Eng.* **1994**, *36*, 25.
(13) Adams, C. R.; Jennings, T. J. *J. Catal.* **1970**, *17*, 157.
(14) Haber, J.; Wojciechowska, M.; Gut, W. *Bull. Pol. Acad. Sci. Chem.* **1996**, *44*, 55.
(15) Collart, O.; Van Der Voort, P.; Vansant, E. F.; Desplantier, D.; Galarneau, A.; Di Renzo, F.; Fajula, F. *J. Phys. Chem. B* **2001**, *105*, 12771.
(16) Van Bavel, E.; Cool, P.; Aerts, K.; Vansant, E. F. *J. Phys. Chem. B* **2004**, *108*, 5263.
(17) Schmidt-Winkel, P.; Lukens, W. W.; Zhao, D.; Yang, P.; Chmelka, B. F.; Stucky, G. D. *J. Am. Chem. Soc.* **1999**, *121*, 254.
(18) Kim, S. S.; Karkamkar, A.; Pinnavaia, T. J.; Kruk, M.; Jaroniec, M. *J. Phys. Chem. B* **2001**, *105*, 7663.
(19) Bordiga, S.; Buzzoni, R.; Geobaldo, F.; Lamberti, C.; Giamello, E.; Zecchina, A.; Leofanti, G.; Petrini, G.; Tozzolo, G.; Vlaic, G. *J. Catal.* **1996**, *158*, 486.
(20) Pérez-Ramírez, J.; Kapteijn, F.; Brückner, A. *J. Catal.* **2003**, *218*, 234.
(21) Yu, Y.; Xiong, G.; Li, C.; Xiao, F. S. *J. Catal.* **2000**, *194*, 487.
(22) Brückner, A.; Lück, R.; Wieker, W.; Fahlke, B.; Mehner, H. *Zeolites* **1992**, *15*, 380.
(23) de Carvalho, M. C. N. A.; Passo, F. B.; Schmal, M. *Appl. Catal. A* **2000**, *193*, 265.
(24) Mendes, F. M. T.; Schmal, M. *Appl. Catal. A* **1997**, *151*, 393.
(25) Ramakrishna Prasad, M.; Kamalakar, G.; Kulkarni, S. J.; Raghavan, K. V. *J. Mol. Catal. A* **2002**, *180*, 109.
(26) Velu, S.; Suzuki, K.; Okazaki, M.; Kapoor, M. P.; Osaki, T.; Ohashi, F. *J. Catal.* **2000**, *194*, 373.
(27) Shimokawabe, M.; Asakawa, H.; Takezawa, N. *Appl. Catal.* **1990**, *59*, 45.
(28) Centi, G.; Perathoner, S.; Biglino, D.; Giamello, E. *J. Catal.* **1995**, *151*, 75.
(29) Neri, G.; Pistone, A.; De Rossi, S.; Rombic, E.; Milone, C.; Galvagno, S. *Appl. Catal. A* **2004**, *260*, 75.
(30) Gaspar, A. B.; Brito, J. L. F.; Dieguez, L. C. *J. Mol. Catal. A* **2003**, *203*, 251.